Simulations of the electrical system of a grid connected marine current energy converter

Christoffer Fjellstedt, Johan Forslund and Karin Thomas

Abstract—**This paper presents a simulation model of the grid connection system for a marine current energy converter deployed in the river Dal (Dalälven) at Söderfors, Sweden. The implementation of the model is done in MATLAB/Simulink. The experimental station consists of a five-bladed turbine connected to a permanent magnet synchronous generator (PMSG) and a bidirectional back-to-back (B2B) converter for the grid connection. The generator side of the electrical system consists of a 2-level voltage source converter (2L-VSC). The generator side converter is controlled using field oriented control (FOC) with zero d-axis current. The grid side converter is a 3-level cascaded H-bridge voltage source converter (3L-CHBVSC) and is controlled using voltage oriented control (VOC) with phase-locked loop (PLL). Simulations are run for constant water speeds as well as for stepwise increases of the speed and for real water speeds from the test site. The controllers are confirmed to be able to correctly control the system for the simulated cases. The power losses are evaluated using steady state simulations and the relative power losses are shown to be smallest for a water speed of around 1.30 m/s. The largest contribution to the total losses is shown to be from the generator.**

Index Terms—**Back-to-back converter, grid connection, hydrokinetic energy, marine current energy converter, three-level cascaded H-bridge converter, two-level converter, vertical axis turbine.**

I. Introduction

THE growing demand for electricity from renewable energy sources has increased the interest in using the energy in unregulated rivers, tides and other marine currents for the generation of electricity. The techniques for using marine currents for electrical power generation are still being actively developed by universities and private enterprises. Therefore, a wide variety of techniques are still being considered. Several different concepts for marine current turbines can be found in [1] and in [2] recent developments in marine current energy projects with large turbines, mainly rated above 500 kW, are presented. An important research area in most renewable energy projects, and also in the development of marine current energy conversion systems, is the design of the electrical system and the control system. The electrical system is used to control the marine current energy converter, for example, to optimize power extraction. It is also the electrical system that enables grid connection. The intermittent character of renewable energy presents a challenge in the design of the grid connection. The character of the specific energy source will also constrain the design of the electrical system. An overview of issues regarding the interaction between marine energy resources, including marine current energy, and the grid are presented in [3]. In [4] grid integration of marine energy converters is discussed based on grid code requirements and experiences from offshore wind power. It can be possible to extrapolate from wind power applications for the design of electrical systems for marine current energy converters. However, the unique requirements for marine current power can make it necessary to construct solutions specifically adapted for marine current energy conversion [4]. Therefore, it is of interest to study electrical systems and control systems for specific marine current energy conversion concepts.

The Marine Current Power Group at Uppsala University deployed an experimental hydro-kinetic power station in 2013 in the river Dal (Dalälven) at Söderfors, Sweden [5]. The experimental station comprises a five-bladed turbine, a permanent magnet synchronous generator and a measurement cabin on shore (housing control and measurement systems). The turbine is illustrated in Figure 1. The grid connection system at the experimental station is mainly based on a back-to-back converter technology, which has been simulated and verified in a laboratory environment [6].

The grid connection system has been experimentally tested on-site and the result of the experiments is that the grid connection system is not working satisfactorily in injecting power into the grid [7]. To further investigate the stability issues with the grid connection this paper presents a simulation model developed in MATLAB/Simulink for the actual turbine deployed at the Söderfors experimental site. The dynamics of the developed model are shown in steady state simulations, simulations with step responses and simulations with real water speed data from the experimental station. The model is also used to estimate the power losses in the system.

II. Turbine and generator

In the following sections, a brief overview of the turbine and the generator is presented. In Table I

Submission ID: 1947, Conference track: Grid integration, PTO & control. The work was supported by STandUP for Energy.

Christoffer Fjellstedt is with the Division of Electricity, Department of Electrical Engineering at Uppsala University, Ångströmlaboratoriet, Lägerhyddsvägen 1, 752 37 Uppsala, Sweden (e-mail: christoffer.fjellstedt@angstrom.uu.se).

Johan Forslund is with the Division of Electricity, Department of Electrical Engineering at Uppsala University, Ångströmlaboratoriet, Lägerhyddsvägen 1, 752 37 Uppsala, Sweden (e-mail: johan.forslund@angstrom.uu.se).

Karin Thomas is with the Division of Electricity, Department of Electrical Engineering at Uppsala University, Ångströmlaboratoriet, Lägerhyddsvägen 1, 752 37 Uppsala, Sweden (e-mail: karin.thomas@angstrom.uu.se).

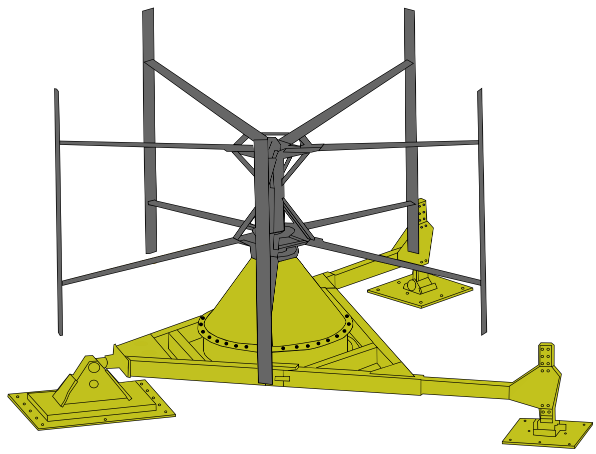

Fig. 1. The Marine current power unit with a vertical axis turbine and generator mounted on the same axis, placed on the riverbed [5]. Illustration by Anders Nilsson.

TABLE I
TURBINE AND GENERATOR PARAMETERS

Turbine	
$C_p(\lambda_{opt})$	0.26 at $\lambda_{opt} = 3.05$
Type	Vertical axis
Rotor height	3.5 m
Rotor radius (r)	3 m
Turbine area (A)	21 m^2
Generator	
Type	Permanent Magnet Synchronous Generator
Power rating	7.5 kW
Nominal rotational speed	15 rpm
Minimum efficiency	80 %
Number of poles	112
Rated voltage ($V_{LL,rms}$)	138 V
Rated stator current (rms)	31 A
Stator phase resistance	0.335 Ω
Armature inductance	3.5 mH
Flux linkage[b,c]	1.29 Wb
Inertia[c]	2445 kgm^2
Viscous friction coefficient[c]	1 Nms

[b] Assuming a constant flux.
[c] The values for flux linkage, inertia and viscous friction are estimates.

the turbine and generator parameters are listed. The nominal values of the turbine and generator can be found in [8] and [9].

A. Turbine

The fraction of power the turbine can capture from the free-flowing water is described by the power coefficient C_p and can be written as

$$C_p = \frac{P_{turbine}}{P_{water}} \tag{1}$$

The power of the free flowing water that interacts with the turbine is

$$P_{water} = \frac{1}{2} A \rho v_w^3 \tag{2}$$

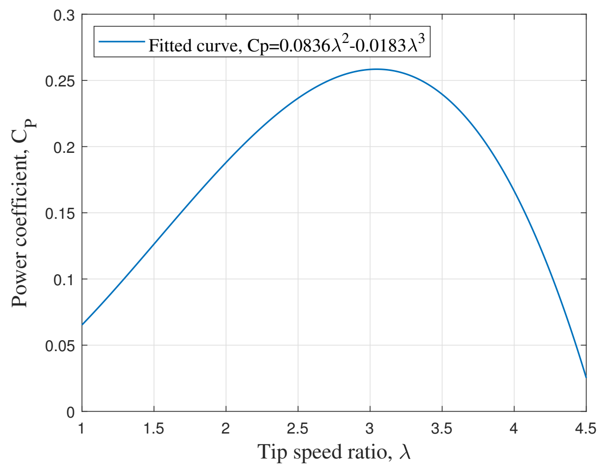

Fig. 2. Power coefficient (C_p) curve fitted from measurements. Optimal tip speed ratio derived from the fitted curve is $\lambda_{opt} \approx 3.05$, which corresponds to an optimal power coefficient of $C_p(\lambda_{opt}) \approx 0.26$.

where A is the area of the turbine, ρ is the density of the water and v_w is the velocity of the water. The area of a vertical axis turbine is given by the diameter times the height of the turbine. The power of the turbine is described by the power of a rotating body $P_{turbine} = \omega_t T_M$, where ω_t is the angular speed of the turbine and T_M is the torque.

The power coefficient is a function of the tip speed ratio (usually denoted TSR or λ) and is defined as the ratio between the tangential speed of the tip of the turbine blade and the velocity of the free-flowing water:

$$\lambda = \frac{\omega_t r}{v_w} \tag{3}$$

The $C_p(\lambda)$-curve has been experimentally verified for TSR values from 2.9-4.5 in flow velocities ranging from 1.2-1.4 m/s in [10]. The curve fitted from the experimental data can be seen in Figure 2 and is given by the following equation

$$C_p(\lambda) = 0.0836\lambda^2 - 0.0183\lambda^3 \tag{4}$$

The optimal tip speed ratio derived from the power coefficient curve is $\lambda_{opt} \approx 3.05$, which gives an optimal power coefficient of $C_p(\lambda_{opt}) \approx 0.26$.

B. Generator

The generator deployed at the experimental site is a 112 pole, cable-wound non-salient permanent magnet synchronous generator (PMSG). The generator is rated at 7.5 kW, 138 $V_{LL,rms}$ at a nominal speed of 15 rpm. The generator and turbine are mounted on the same shaft without a gearbox. Therefore, the angular speed of the generator is the same as the angular speed of the turbine. The generator parameters are listed in Table I. The design and development of the generator are described in more detail in [11] and [12].

III. Electrical and Control System

The following sections present the basics of the electrical system at the Söderfors experimental station. More details about the design can be found in [13].

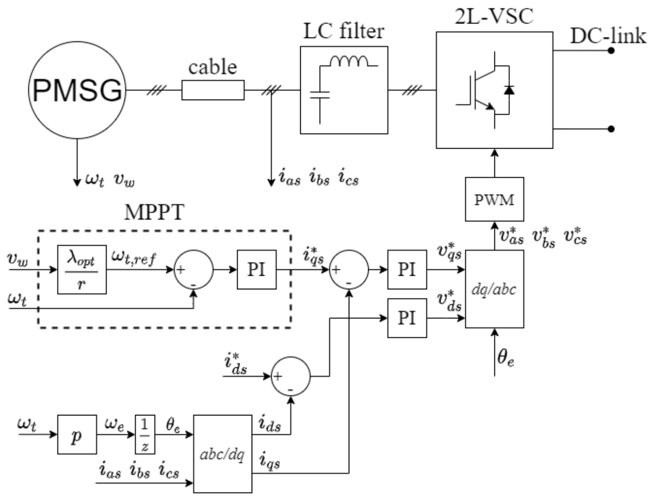

Fig. 3. Generator side electrical and control system.

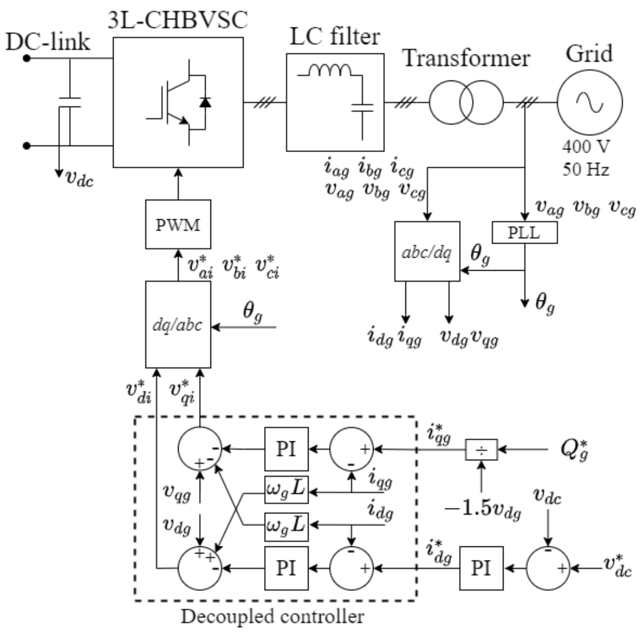

Fig. 4. Grid side electrical and control system.

A. Overview

The generator side and grid side of the electrical system is presented in Figure 3 and Figure 4, respectively. In both Figures, essential parts of the control system are included. The AC voltage from the generator is converted with a 2-level voltage source converter (2L-VSC) to a DC-link. The input to the 2L-VSC converter is filtered with a harmonic LC filter. Together with the inductance of the stator windings of the generator, this forms an LCL filter. The converter is controlled using field-oriented control (FOC) with zero d-axis current coupled with a maximum power point tracking (MPPT) control scheme to achieve maximum active power extraction from the turbine. The DC-link consists of a capacitor and connects to a 3-level cascaded H-bridge voltage source converter (3L-CHBVSC) used to enable grid connection. The 3L-CHBVSC is controlled using a voltage oriented control (VOC) method together with a phase-locked loop (PLL) scheme used to synchronize the converter controller with the grid. The 3L-CHBVSC is connected to a wye-delta transformer via an LC filter, which together with the inductance of the transformer forms an LCL filter. Both the 2L-VSC and 3L-CHBVSC are bidirectional, meaning that the converters can be operated in both rectifying and inverting mode. The main focus of this article is on the power transfer from the turbine to the grid. Therefore, the 2L-VSC will be operated as a rectifier and the 3L-CHBVSC will be operated as an inverter. This type of system topology is often called a back-to-back (B2B) converter and the implementation and control are thoroughly described in [14] and [15].

TABLE II
ELECTRICAL SYSTEM PARAMETERS

Component	Parameters	Values
Cable	Length	∼200 m
	Resistance	0.08 Ω[a]
Rectifier	Converter type	2L-VSC
	Modulation scheme	SPWM
	Switching frequency	4 kHz
	Harmonic LC filter	1.6 mH, 10 μF
DC-link filter	Capacitor bank	16.5 mF
Inverter	Converter type	3L-CHBVSC
	Modulation scheme	SPWM
	Switching frequency	6 kHz
	Harmonic LC filter	3.1 mH, 10 μF
Transformer	Wye/Delta	340 V/400 V
	Power rating	7.5 kVA
	Primary resistance	180 mΩ
	Secondary resistance	230 mΩ
	Primary leak. inductance	0.52 mH
	Seconday leak. inductance	0.37 mH
	Magnetization resistance	360 Ω[b]
	Magnetization inductance	3.23 H[b]
Grid	Three-phase symetrical	400 V/50 Hz
IGBT	Internal resistance	0.1 mΩ
	Forward voltage	1 V
Rectifier diode	Internal resistance	0.001 Ω
	Forward voltage	0.8 V
Snubber circuit	Snubber resistance	47 kΩ
	Snubber capacitance	470 nF

The Table is partly adapted from Table 2 in [13].
[a] Measured value.
[b] Calculated from measurements on the transformer.

B. Control of generator side converter

The MPPT scheme is implemented to control the angular speed of the turbine in order to achieve optimal TSR. Since the optimal TSR corresponds to the peak value of the power coefficient, the power extracted from the turbine is maximized when the turbine operates at an angular speed which corresponds to the optimal TSR for the actual water speed. As can be seen in Figure 3, the input to the MPPT block is the angular speed of the turbine and the water speed. The block uses equation 3 to calculate a reference value for the angular speed of the turbine, ω_{ref}.

The PMSG is controlled using FOC. In this method, the generator phase currents i_{as}, i_{bs} and i_{cs} are transformed into a rotating coordinate system with a dq transform. The dq-axis currents i_{ds} and i_{qs} are then used to control the generator. In the method implemented here, the d-axis current is maintained at zero, $i_{ds} = 0$, and by doing this the q-axis current i_{qs} becomes equal to the stator current of the generator. The electromagnetic torque of the generator is then given by

$$T_e = \frac{3}{2} p \lambda_r i_{qs} \tag{5}$$

where p is the number of pole pairs and λ_r is the rotor flux linkage. If the rotor flux linkage is assumed to be constant, the relationship between the electromagnetic torque and the stator current is linear.

The control strategy in the FOC method implemented here consists of three PI controllers, as can be seen in Figure 3. The inner loop consists of two PI controllers for the dq-axis currents and one outer loop for rotor speed. The dq frame of reference needs to be synchronized with the generator. Therefore, the turbine speed is measured, multiplied with the pole pairs to attain the electrical angular speed of the generator and integrated, which gives the angular position (θ_e) of the rotating frame of reference.

The reference value of the angular speed of the turbine $\omega_{t,ref}$ is compared with the measured angular speed ω_t (in the simulations in this article the electrical angular speed was used). The error is sent to the rotor speed PI controller. The output from this controller is the reference q-axis current i^*_{qs}, which is compared with the measured current i_{qs}. The measured d-axis current is compared with the reference $i^*_{ds} = 0$ and the errors are sent to the inner loop PI controllers. The output from the current PI controllers are the reference dq-axis voltages v^*_{ds} and v^*_{qs}. These voltages are then transformed back to the stationary frame of reference and the voltages v^*_{as}, v^*_{bs} and v^*_{cs} are used as reference signals in the pulse width modulation (PWM) generation block. The PWM block uses a carrier-based pulse width modulation technique to generate control pulses for the 2L-VSC.

C. Control of grid side converter

The electrical and control system for the grid side is shown in Figure 4. The grid side converter is controlled using VOC with PLL. The PLL is used to detect the voltage angle θ_g of the grid. This angle is then used for transformations between the stationary abc frame and the synchronous dq frame. The VOC scheme consists of two inner feedback control loops for the control of the dq-axis currents and one outer control loop for the control of the DC-link voltage. The VOC control scheme requires that the d-axis of the synchronous frame is aligned with the grid voltage vector. The magnitude of the d-axis component of the grid voltage will in this case be equal to the magnitude of the grid voltage vector ($v_d = v_{dg}$). Therefore, the resultant q-axis voltage will be zero ($v_{qg} = 0$). The active and reactive power exchanged with the grid can then be expressed with the following equation:

$$\begin{aligned} P_g &= \frac{3}{2}\left(v_{dg} i_{dg} + v_{qg} i_{qg}\right) = \frac{3}{2} v_{dg} i_{dg} \\ Q_g &= \frac{3}{2}\left(v_{qg} i_{dg} - v_{dg} i_{qg}\right) = -\frac{3}{2} v_{dg} i_{qg} \end{aligned} \tag{6}$$

Using equation 6, the reference q-axis current can be calculated by

$$i^*_{qg} = \frac{Q^*_g}{-1.5 v_{dg}} \tag{7}$$

and if the reference reactive power Q^*_g is set to zero unity power factor operation can be achieved.

For a grid connected 3-level inverter with a simple L filter it can be shown (see for example [15, p. 146-148]) that the state equations for the AC side of the inverter can be expressed in the dq frame of reference by the following system of equations:

$$\begin{aligned} L\frac{di_{dg}}{dt} &= \left(v_{dg} - v_{di} + \omega_g L i_{qg}\right) \\ L\frac{di_{qg}}{dt} &= \left(v_{qg} - v_{qi} - \omega_g L i_{dg}\right) \end{aligned} \tag{8}$$

The voltages v_{di} and v_{qi} are the dq transforms of the phase voltages on the AC side of the converter and ω_g is the angular frequency of the grid. For the purpose of the design of the controller, it is assumed that the grid side system can be simplified into a simple L filter connected directly to the grid. Therefore, equation 8 is used to describe the system. The inductance L is assumed to consist of the series connection of the inductance in the LC filter and the primary leakage inductance of the transformer.

As can be observed in equation 8 there is a coupling between the d-axis and the q-axis components by the terms $\omega_g L i_{qg}$ and $\omega_g L i_{dg}$. It is preferable to decouple the dq components, since this enables independent control of the d-axis and the q-axis currents. Therefore, as can be seen in Figure 4, the dq-axis current controller is implemented as a decoupled controller.

As can be seen in Figure 4 the grid voltages v_{ag}, v_{bg} and v_{cg} and grid currents i_{ag}, i_{bg} and i_{cg} are measured. The grid voltages are used in the PLL block to acquire the grid voltage angle θ_g. The grid voltages and grid currents are transformed from the stationary abc frame to the synchronous dq frame using the grid voltage angle as the angular position of the rotating frame of reference. The reference value for the q-axis current is calculated with equation 7 for the desired reference value of the reactive power and sent to the decoupling block. In the simulations the reactive power is set to zero. The reference value for the d-axis current i^*_{dq} is acquired from the outer voltage control loop, in which the DC-link voltage v_{dc} is measured and compared to a set point value v^*_{dc} and the error is sent to a PI controller. The set point value of the DC-link voltage is 400 V. In the decoupled controller the reference dq-axis currents are compared to the measured dq-axis currents and the error is sent to the inner loop PI controllers. The output from the decoupled controller block are the reference voltages v^*_{di} and v^*_{qi}, which are transformed into the stationary frame of reference. The reference voltages v_{ai}^*, v_{bi}^* and v_{ci}^* are then used as reference signals in the PWM block, where a sinusoidal carrier-based method is used to generate control pulses for the converter.

IV. Implementation of model in MATLAB/Simulink

The generator side and grid side electrical and control system in Figure 3 and Figure 4, respectively, are implemented as one model in MATLAB/Simulink. The model is implemented using built-in blocks and functions in Simulink for the different parts of the systems. The parameters used in the simulations are listed in Table I and II. The power coefficient curve in equation 4 is implemented as a mathematical function. The PI controllers are implemented as discrete-time parallel controllers. The PI controller in the voltage control loop is additionally supplemented with an anti-windup scheme. The DC-link and the passive components are assumed to be lossless.

The system is simulated in discrete time. The electrical components are sampled at a time step of 0.5 μs. The other components in the system are sampled at a time step defined automatically by Simulink. The solver is a variable-step solver automatically selected by Simulink.

V. Simulation results and discussion

In the following sections the results from simulations of the system are presented and discussed. Firstly, the performance of the implemented control system in steady state is presented. Then, the dynamics of the system is further evaluated by simulations with varying water speeds in the form of step changes in the water speed and simulations with real water speed data from the experimental test site in Söderfors. Lastly, the power losses in the system are presented.

A. Simulation of the system in steady state

The performance of the control system in steady state was tested by simulating the system for 6 seconds with a water speed of 1.35 m/s as input. The system was allowed 3 seconds to settle into steady state and data from the last 3 seconds of the simulation was extracted.

The generator side controller should in steady state be able to keep the TSR and power coefficient at their respective optimal values by controlling the angular speed of the turbine. According to equation 3, for a water speed of 1.35 m/s and the optimal TSR of 3.05 the expected angular speed of the turbine and rotor is 1.3725 rad/s. Figure 5 shows the power coefficient (C_p), the TSR, the angular speed of the turbine (ω_t) and the power on the turbine. As can be observed, the angular speed of the turbine is maintained at the expected value with some small ripples. The same observation is valid for the TSR and the power coefficient. It can also be observed that the power on the turbine is maintained at around 6677 W, which is expected if the $C_p(\lambda)$-curve in equation 4, the definition of the power

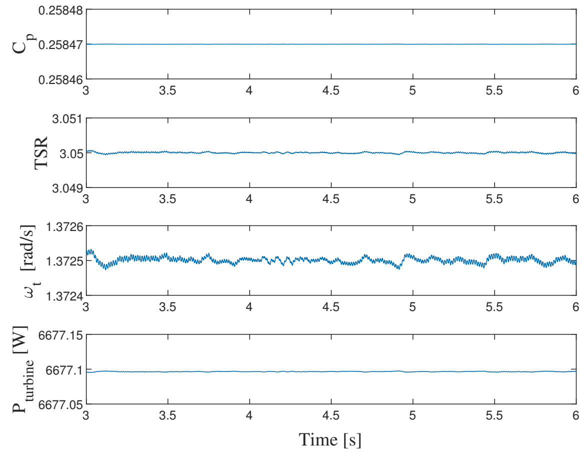

Fig. 5. Power coefficient (C_p), tip speed ratio (TSR), angular speed of the turbine (ω_t) and power on the turbine ($P_{turbine}$) for a steady state simulation with the water speed 1.35 m/s.

coefficient in equation 1, the power in free flowing water in equation 2 and the TSR in equation 3 are used to calculate the power on the turbine for the optimal TSR and the water speed 1.35 m/s. It can therefore be concluded that the generator side controller is able to maintain the system at the optimal values in steady state.

When the generator supplies the system with power, the generator side controller is responsible for maximizing the power extracted by regulating the angular speed of the turbine. The controller of the grid side inverter is supposed to maintain the voltage of the DC-link at a predefined voltage level and transfer all the power, which have been delivered from the generator to the DC-link, to the grid. The grid side controller should also, because of the decoupling, independently regulate the reactive power exchange with the grid to zero. The currents injected into the grid are also supposed to be synchronised with the grid frequency by the PLL block. As can be seen in Figure 6 the DC-link voltage is maintained at the desired 400 V with only minor ripple. The decoupled current controller is able to keep the reactive power exchanged with the grid at an average of zero with some ripple. The active power injected into the grid is on average just below 5000 W. The currents $i_{grid,abc}$ are synchronized with the grid and maintained at a frequency of 50 Hz.

B. Simulation of step changes in water speed

The stability of the electrical system was tested by running it for 20 seconds and using 6 steps in water speed. It takes about one second for the simulation to initially reach a steady state. Each set point was operated for 2 seconds to let the turbine angular speed settle before the next step.

The simulated water speed, the turbine angular speed and the TSR of the turbine during operation can be seen in Figure 7. The TSR has been normalized using the estimated optimal TSR for the turbine, 3.05. The control system is able to make the turbine follow the water speed to keep the turbine operating

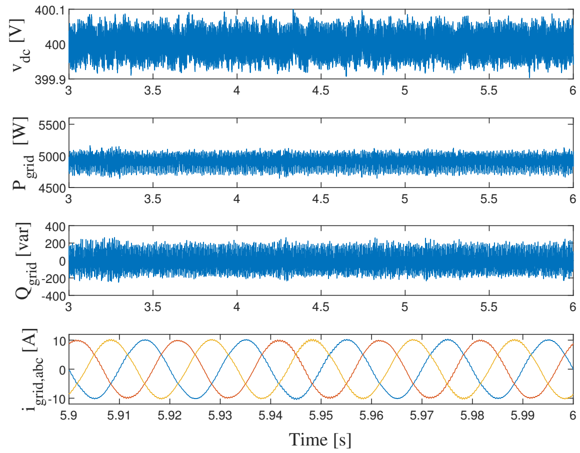

Fig. 6. DC-link voltage (v_{dc}), active power injected into the grid (P_{grid}), reactive power exchanged with the grid (Q_{grid}) and the grid currents ($i_{grid,abc}$). The grid currents are illustrated for a shorter time period.

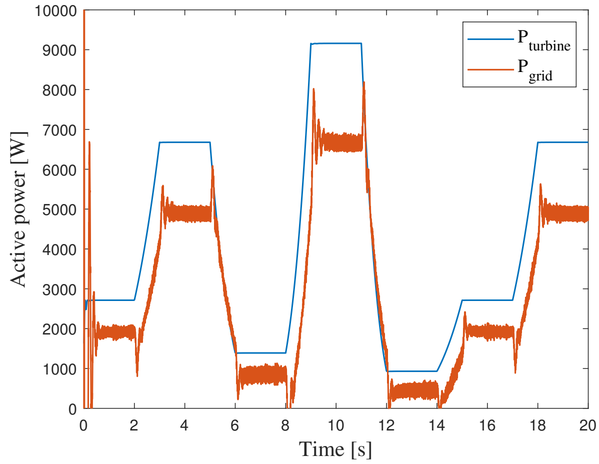

Fig. 8. Mechanical power injected into the generator and electrical power injected into the grid during step responses for simulated changes in water speed.

at optimal TSR during the steps of water speeds. The overshoot in angular speed does not exceed 6 % and the largest deviation from optimal TSR was 5.5 %. The implementation of the turbine angular speed control is fast enough to keep the TSR close to the optimum with a small overshoot. The mechanical power extracted by the turbine and the electrical power injected into the grid can be seen in Figure 8. The implemented grid side current control is able to inject power into the grid when it is available on the DC-link, with small oscillations in power when a step is initiated. The voltage on the DC-link can be seen in Figure 9. The variations in voltage are very small when the water speed is constant, at around 0.025 %. During the steps, the overshoot in voltage did not exceed 1 % of the target value.

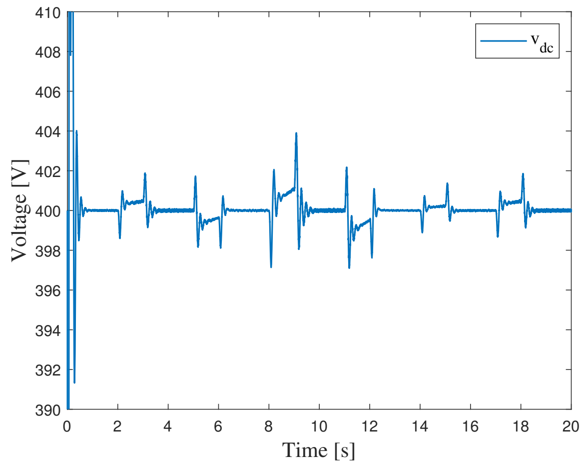

Fig. 9. The voltage on the DC-link during step responses for simulated changes in water speed.

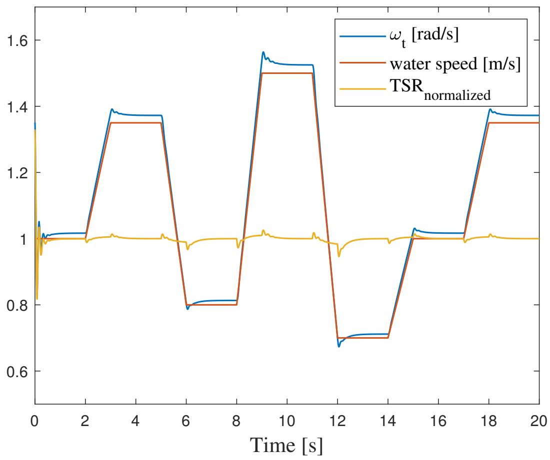

Fig. 7. Turbine angular speed, water speed and TSR for the turbine normalized around the optimum at 3.05, during step responses for simulated changes in water speed.

C. Simulation using measured water speeds

The stability of the electrical system was further tested using measured water speeds from the experimental site in Söderfors.

The simulated water speed, the turbine angular speed and the TSR of the turbine during operation can be seen in Figure 10. The turbine angular speed follows the water speed closely, indicating that the implemented angular speed control is fast enough for optimizing the TSR of the turbine. There is no visible departure from the optimal TSR value, where the maximum difference is 0.1 % from the set point. The mechanical power extracted by the turbine and the electrical power injected into the grid can be seen in Figure 11. The power injected into the grid follows the power extracted by the turbine suggesting that the implemented current control of the grid side converter is appropriate. The voltage on the DC-link can be seen in Figure 12. The voltage is kept very close to the desired value off 400 V, never measuring more than 0.05% away from the set point.

D. Power losses in the system

The power losses in the system were evaluated for 19 different water speeds using simulations of the system.

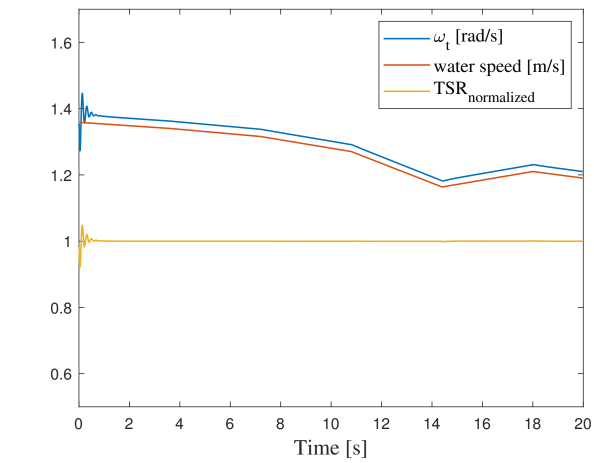

Fig. 10. Turbine angular speed, water speed and TSR for the turbine normalized around the optimum at 3.05, during a simulation using measured water speeds as input to the turbine.

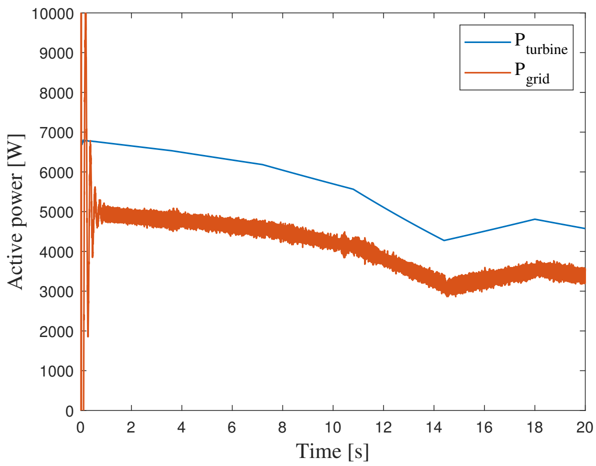

Fig. 11. Mechanical power injected into the generator and electrical power injected into the grid during a simulation using measured water speeds as input to the turbine.

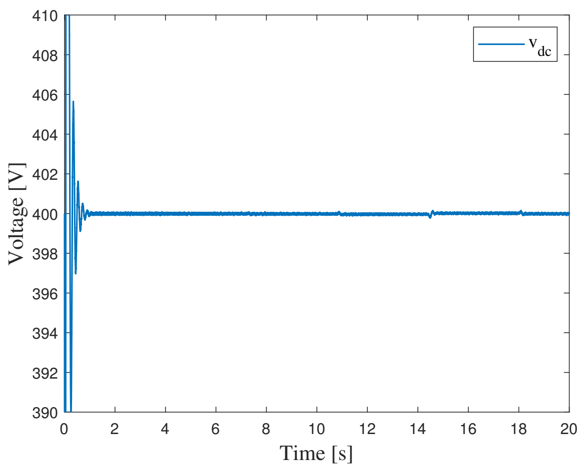

Fig. 12. The voltage on the DC-link during a simulation using measured water speeds as input to the turbine.

The system was allowed to settle into the steady state for each respective water speed and 2 seconds of data were extracted from the simulation. The losses were

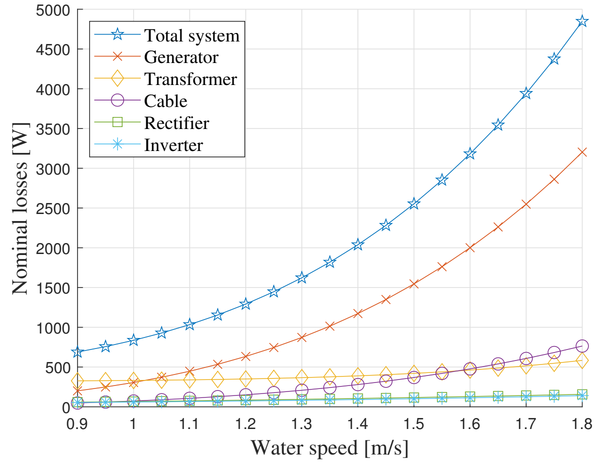

Fig. 13. Nominal power losses of the total system and of different parts of the system in steady state for different water speeds.

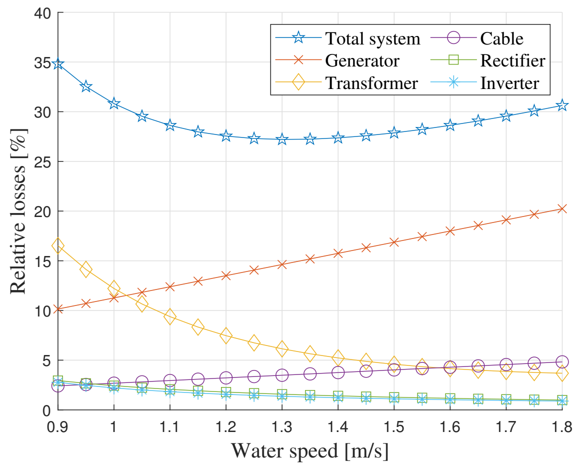

Fig. 14. Relative power losses of the total system and of different parts of the system in steady state for different water speeds. The losses are calculated as relative to the input mechanical power to the generator.

calculated as the average losses for the extracted data. The losses of the rectifier and the inverter has mainly two contributions: switching and conduction losses. The conduction losses are included in the simulations. The switching losses correspond to the energy needed to open and close the IGBTs and are here estimated as a constant contribution to the losses of the rectifier and inverter, respectively. The values of the switching losses are calculated from the manufacturer's specifications for the IGBTs installed in the actual electrical system at the test site. The installed IGBT Modules are 2MBI100TA-060-50 from Fuji. The switching losses of the rectifier and inverter are estimated to 20 W and 30 W, respectively.

Figure 13 shows the nominal total losses of the system and the nominal losses of the generator, the transformer, the cable, the rectifier and the inverter. The losses increase as the water speed increase, which is expected since more power is extracted from the turbine for higher water speeds. When the power increases, the currents in the system become larger and give rise to larger conduction losses. The largest contribution to

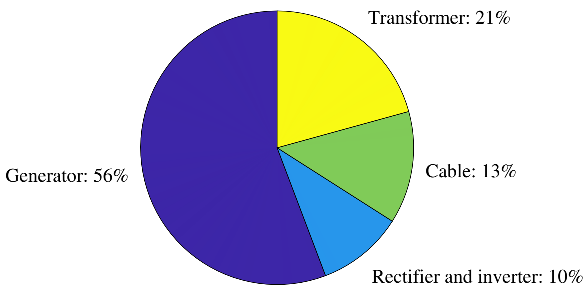

Fig. 15. The relation between the power losses in different parts of the system for the water speed 1.35 m/s.

the total losses is from the generator. The losses in the generator, the cable, the rectifier and the inverter follow the same trend with increasing losses for higher water speeds. On the other hand, the transformer losses increase more slowly. This indicates that the copper losses are a minor contribution in relation to the core losses in the transformer. Since the switching losses are estimated as a constant contribution the increase in losses that can be observed for the rectifier and inverter are only attributable to the conduction losses.

Figure 14 presents the relative losses with regards to the input mechanical power on the generator. As can be observed, the lowest percentage loss occurs around water speeds of 1.3 m/s. The relative losses of the generator and the cables increase for higher water speeds, while the relative losses of the rectifier, the inverter and the transformer decrease. The relative losses of the transformer decrease more rapidly compared to the relative losses of the rectifier and inverter. This can be understood if Figure 13 is observed where, as noted above, the losses of the transformer increase more slowly compared with the losses of the rectifier and the inverter.

Finally, Figure 15 illustrates the relation between the losses in different parts of the system for the water speed 1.35 m/s. As is clearly visible the most significant contribution to the losses is from the generator. The losses in the converters have the least significant impact on the system. It should be noted that since both the generator losses and the cable losses increase more rapidly compared with the transformer losses, the relative significance of the losses in these parts of the system will become more significant for higher water speeds.

Since the losses of the system significantly can be deduced to copper losses in the generator, attempts to increase the efficiency of the system could with advantage be focused on reducing the losses in the generator.

VI. Conclusion

A simulation model for a B2B grid connection system for a marine current energy converter deployed in the river Dal (Dalälven) at Söderfors, Sweden, has been developed in MATLAB/Simulink. The dynamics and performance of the system have been investigated by simulations. The simulation results have shown that the generator side controller is able to achieve optimal power extraction from the water. The grid side inverter is able to inject power into the grid while maintaining the voltage level of the internal DC-link and not exchanging reactive power with the grid. The simulation results have further shown that the system can handle step changes in the water speed as well as simulations with real water speed data from the Söderfors experimental site. The losses in the system have been evaluated for different water speeds using steady state simulations. The relative losses of the total system are lowest for a water speed of around 1.30 m/s and the most significant contribution to the total power losses is from the generator.

Acknowledgement

The work was supported by STandUP for Energy.

References

[1] J. Zhang, L. Moreau, M. Machmoum, and P.-E. Guillerm, "State of the art in tidal current energy extracting technologies," in *2014 First International Conference on Green Energy ICGE*, 2014, pp. 1–7.

[2] Z. Zhou, M. Benbouzid, J.-F. Charpentier, F. Scuiller, and T. Tang, "Developments in large marine current turbine technologies - a review," *Renewable & sustainable energy reviews*, vol. 71, pp. 852–858, 2017.

[3] J. Khan, G. Bhuyan, A. Moshref, K. Morison, J. H. Pease, and J. Gurney, "Ocean wave and tidal current conversion technologies and their interaction with electrical networks," in *2008 IEEE Power and Energy Society General Meeting - Conversion and Delivery of Electrical Energy in the 21st Century*. IEEE, 2008, pp. 1–8.

[4] M. Santos-Mugica, E. Robles, A. G. Endegnanew, E. Tedeschi, and J. Giebhardt, "Grid integration and power quality testing of marine energy converters: Research activities in the marinet project," in *2014 Ninth International Conference on Ecological Vehicles and Renewable Energies (EVER)*. IEEE, 2014, pp. 1–9.

[5] S. Lundin, J. Forslund, N. Carpman, M. Grabbe, K. Yuen, S. Apelfröjd, A. Goude, and M. Leijon, "The Söderfors project: Experimental hydrokinetic power station deployment and first results," in *Proceedings of the 10th European Wave and Tidal Energy Conference, EWTEC13, Aalborg, Denmark*, 2–5 September 2013.

[6] S. Apelfröjd, K. Thomas, and M. Leijon, "Experimental verification of a back-to-back 2l-3l grid connection system for a marine current energy converter," in *2nd International Conference on Offshore Renewable Energy (CORE16), Glasgow, UK*, September 2016, pp. 294–299.

[7] J. Forslund and K. Thomas, "First Experimental Results of a Grid Connected Vertical Axis Marine Current Turbine using a Multilevel Power Converter," in *Proceedings of the 4th Asian Wave and Tidal Energy Conference, AWTEC18, Taipei, Taiwan*, September 2018.

[8] M. Grabbe, K. Yuen, A. Goude, E. Lalander, and M. Leijon, "Design of an experimental setup for hydro-kinetic energy conversion," *International Journal on Hydropower & Dams*, vol. 15, no. 5, pp. 112–116, 2009.

[9] K. Yuen, S. Lundin, M. Grabbe, E. Lalander, A. Goude, and M. Leijon, "The Söderfors project: Construction of an experimental hydrokinetic power station," in *Proceedings of the 9th European Wave and Tidal Energy Conference, EWTEC11, Southampton, UK*, 5-9 September 2011, pp. 1–5.

[10] S. Lundin, J. Forslund, A. Goude, M. Grabbe, K. Yuen, and M. Leijon, "Experimental demonstration of performance of a vertical axis marine current turbine in a river," *Journal of Renewable and Sustainable Energy*, vol. 8, no. 6, pp. 064 501–1–5, 2016.

[11] M. Grabbe, K. Yuen, S. Apelfröjd, and M. Leijon, "Efficiency of a directly driven generator for hydrokinetic energy conversion," *Advances in Mechanical Engineering*, vol. 2013, pp. 1–8, 2013, article ID 978140.

[12] M. Grabbe, S. Eriksson, and M. Leijon, “On the stator slot geometry of a cable wound generator for hydrokinetic energy conversion,” *The Scientific World Journal*, vol. 2015, pp. 1–6, 2015, article ID 812149.

[13] S. Apelfröjd, R. Ekström, K. Thomas, and M. Leijon, “A back-to-back 2L-3L grid integration of a marine current energy converter,” *Energies*, vol. 8, pp. 808–820, January 2015.

[14] A. Yazdani and R. Iravani, *Voltage-sourced converters in power systems: modeling, control, and applications*, 1st ed. Hoboken, N.J: IEEE Press/John Wiley, 2010.

[15] B. Wu, Y. Lang, N. Zargari, and S. Kouro, *Power conversion and control of wind energy systems*, 1st ed. NJ, Hoboken: IEEE Press, 2011, vol. 77.